

X-ray isophote shapes and the mass of NGC 3923

David A. Buote¹ and Claude R. Canizares²

¹*Institute of Astronomy, Madingley Road, Cambridge CB3 0HA*

²*Department of Physics and Center for Space Research 37-241, Massachusetts Institute of Technology, 77 Massachusetts Avenue, Cambridge, MA 02139, U.S.A.*

12 June 2018

ABSTRACT

We present analysis of the shape and radial mass distribution of the E4 galaxy NGC 3923 using archival X-ray data from the *ROSAT* PSPC and HRI. The X-ray isophotes are significantly elongated with ellipticity $\epsilon_x = 0.15(0.09 - 0.21)$ (90% confidence) for semi-major axis $a \sim 10h_{70}^{-1}$ kpc and have position angles aligned with the optical isophotes within the estimated uncertainties. Applying the Geometric Test for dark matter, which is independent of the gas temperature profile, we find that the ellipticities of the PSPC isophotes exceed those predicted if $M \propto L$ at a marginal significance level of 85%(80%) for oblate (prolate) symmetry. Detailed hydrostatic models of an isothermal gas yield ellipticities for the gravitating matter, $\epsilon_{mass} = 0.35 - 0.66$ (90% confidence), which exceed the intensity weighted ellipticity of the *R*-band optical light, $\langle \epsilon_R \rangle = 0.30$ ($\epsilon_R^{max} = 0.39$).

We conclude that mass density profiles with $\rho \sim r^{-2}$ are favored over steeper profiles if the gas is essentially isothermal (which is suggested by the PSPC spectrum) and the surface brightness in the central regions ($r \lesssim 15''$) is not modified substantially by a multi-phase cooling flow, magnetic fields, or discrete sources. We argue that these effects are unlikely to be important for NGC 3923. (The derived ϵ_{mass} range is very insensitive to these issues.) Our spatial analysis also indicates that the allowed contribution to the *ROSAT* emission from a population of discrete sources with $\Sigma_x \propto \Sigma_R$ is significantly less than that indicated by the hard spectral component measured by *ASCA*.

Key words: galaxies: elliptical and lenticular, cD – galaxies: fundamental parameters – galaxies: individual (NGC 3923) – galaxies: structure – X-rays: galaxies.

1 INTRODUCTION

The structure of the dark matter halos of galaxies provides important clues to their formation and dynamical evolution (e.g. Sackett 1996; de Zeeuw 1996, 1997). For example, in the Cold Dark Matter (CDM) scenario (e.g. Ostriker 1993) there is evidence that the density profiles of halos have a universal form essentially independent of the halo mass or Ω_0 (Navarro, Frenk, & White 1997; though see Moore et al. 1997). The intrinsic shapes of CDM halos are oblate-triaxial with ellipticities similar to the optical isophotes of elliptical galaxies (e.g. Dubinski 1994). The global shape of a halo also has implications for the mass of a central black hole (e.g. Merritt & Quinlan 1997).

At present accurate constraints on the intrinsic shapes and density profiles of early-type galaxies are not widely

available (e.g. Sackett 1996; Olling & Merrifield 1997)*. Stellar dynamical analyses that have incorporated the information contained in high order moments of stellar velocity profiles have made important progress in limiting the uncertainty in the radial distribution of gravitating mass arising from velocity dispersion anisotropy (Rix et al. 1997; Gerhard et al. 1997). However, as indicated by the paucity of such stellar dynamical measurements, the required observations to obtain precise constraints at radii larger than $\sim R_e$ are extensive, and the modeling techniques to recover the phase-space distribution function are complex. It is also unclear whether this method can provide interesting constraints on the intrinsic shapes since only weak limits on the range of possible shapes have been obtained from analysis of velocity profiles out to $\sim 2 R_e$ (e.g. Statler 1994).

* The distribution of dark matter in spiral galaxies is also far from being a solved problem – see, e.g. Broeils (1997).

Interesting measurements of the ellipticity of the gravitating mass have been obtained for two Polar Ring galaxies (Sackett et al. 1994; Sackett & Pogge 1995) and from statistical averaging of known gravitational lenses (e.g. Keeton, Kochanek, & Falco 1997), but owing to the rarity of these objects it is possible that the structures of their halos are not representative of most early-type galaxies. Moreover, gravitational lenses, which are biased towards the most massive galaxies, only give relatively crude constraints on the ellipticity and radial mass distribution for any individual system and only on scales similar to the Einstein radius (e.g. Kochanek 1991).

The X-ray emission from hot gas in isolated early-type galaxies (Forman, Jones, & Tucker 1985; Trinchieri, Fabbiano, & Canizares 1986; for a review see Sarazin 1997) probably affords the best means for measuring the shapes and radial mass distributions in these systems (for a review see Buote & Canizares 1997b; also see Schechter 1987 and the original application to the analogous problem of the shapes of galaxy clusters by Binney & Strimple 1978). The isotropic pressure tensor of the hot gas in early-type galaxies greatly simplifies measurement of the mass distribution over stellar dynamical methods. Moreover, since the shape of the volume X-ray emission traces the shape of the gravitational potential independent of the (typically uncertain) gas temperature profile (Buote & Canizares 1994, 1996a), the shape of the mass distribution can be accurately measured in a way that is quite robust to the possible complicating effects of multi-phase cooling flows and magnetic fields (see Buote & Canizares 1997b).

Presently, X-ray measurements of the mass distributions in early-type galaxies are inhibited by limitations in the available data. The *ROSAT* (Trümper 1983) Position Sensitive Proportional Counter (PSPC) (Pfeffermann et al. 1987) has inadequate spatial resolution (PSF $\sim 30''$ FWHM) to map the detailed mass distributions for all but the largest nearby galaxies, and the limited spectral resolution and band width complicates interpretation of the measured temperature profiles (Buote & Canizares 1994; Trinchieri et al. 1994; Buote & Fabian 1997). Although equipped with superior spatial resolution (PSF $\sim 4''$ FWHM), the *ROSAT* High Resolution Imager (HRI) (David et al. 1997) has too small an effective area and too large an internal background to provide images of sufficient quality for many galaxies for radii $r \gtrsim R_e$. Among the few galaxies with detailed measurements of their radial mass profiles are NGC 507 (Kim & Fabbiano 1995), NGC 1399 (Rangarajan et al. 1995; Jones et al. 1997), NGC 4472 (Irwin & Sarazin 1996), NGC 4636 (Trinchieri et al. 1994), NGC 4649 (Brighenti & Mathews 1997), and NGC 5044 (David et al. 1994).

The shape of the gravitating mass has been measured via X-ray analysis for the E4 galaxy NGC 720 and the E7/S0 galaxy NGC 1332 and found to be at least as elongated as the optical isophotes (Buote & Canizares 1994, 1996a, 1997a). For NGC 720, which has more precise constraints, the ellipticity of the gravitating matter is $\epsilon_{mass} = 0.44-0.68$ (90% confidence) compared to the intensity weighted ellipticity of the optical light, $\langle \epsilon \rangle = 0.31$ (Buote & Canizares 1997a). In addition, the X-ray isophotes of NGC 720 twist from being aligned with the optical isophotes within R_e to a position $\sim 30^\circ$ offset at larger radii. This twist, when combined with the ellipticities of the X-ray isophotes, cannot

be explained by the projection of a reasonable triaxial matter distribution and thus may implicate a dark matter halo misaligned from the stars (Buote & Canizares 1996b; Romanowsky & Kochanek 1997).

NGC 720 and NGC 1332 were selected for analysis since they are isolated, significantly elongated in the optical, sufficiently bright, and sufficiently dominated by emission from hot gas in the *ROSAT* band. In this paper we present X-ray analysis of the classic “shell” galaxy, NGC 3923, which is the last galaxy of which we are aware that satisfies these selection criteria and has deep *ROSAT* observations. This isolated E4 galaxy has both archival *ROSAT* PSPC and HRI data and its *ASCA* spectrum has been analyzed previously (Buote & Fabian 1997). This will serve as our final case study until the impending launch of *AXAF* revolutionizes this field.

The organization of this paper is as follows. In §2 we describe the *ROSAT* observations and the data reduction. We discuss removal of point sources in §3. Measurements of the ellipticities of the X-ray isophotes and the radial profiles are described in §4 and §5 respectively. Analysis of the PSPC spectrum is presented in §6. We give results for the Geometric Test for dark matter in §7 and constraints on the shape and radial mass distribution from detailed hydrostatic models in §8. Finally, in §9 we give our conclusions.

2 OBSERVATIONS AND DATA REDUCTION

2.1 PSPC

NGC 3923 was observed with the PSPC for 14.5 ks from 17-19 December 1991 and for 24 ks from 23-26 June 1993. Both observations were positioned at the field center where the point spread function is smallest. Since spatial resolution is of principal importance for our analysis of the shape of the X-ray surface brightness, we analyze only the PSPC data in the hard band (PI channels 42-201, $E \approx 0.4 - 2.0$ keV) to further optimize the size of the PSF; for details regarding the PSPC PSF see Hasinger et al. (1993, updated 1994) and see Aschenbach (1998) for a description of the *ROSAT* X-ray telescope.

We reduced each observation separately with the standard XSELECT, FTOOLS, and IRAF-PROS software. Firstly, the events files were cleaned of after-pulse signals by removing any events following within 0.35 ms of a precursor. We then removed large fluctuations in the light curves indicative of scattered light from the Bright Earth, Sun, or SAA; this resulted in filtered exposures of 13.5 ks for the 1991 observation and 21.8 ks for the 1993 observation.

To optimize signal-to-noise (S/N) and bin-size requirements for computing ellipticities (see §4), we binned the cleaned events files into images with $5''$ pixels. Exposure maps for the appropriate energy band (PI=42-201) were then generated for each image and were then used to create flattened images; note that the intrinsic resolution of the exposure maps is $15''$. Finally, we aligned the images using bright point sources in the field and then combined the images. The final image is displayed in Figure 1

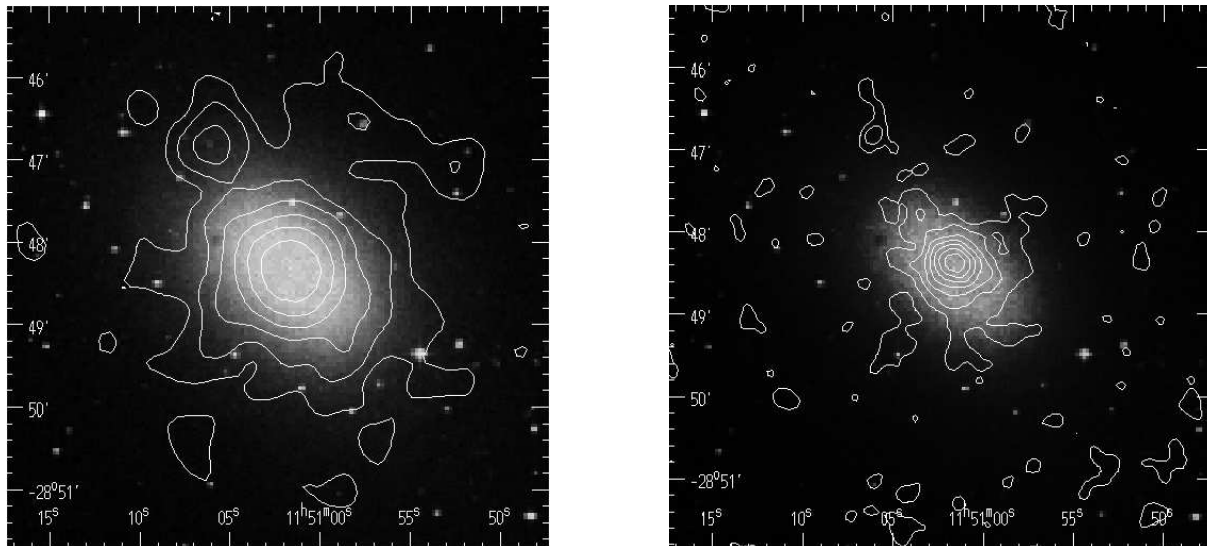


Figure 1. Reduced images of the PSPC (left) and HRI (right) observations overlaid on the digitized POSS images. Each X-ray image has been smoothed with a Gaussian ($\sigma = 5''$) for visual clarity, although the images used for analysis have not been smoothed as such.

2.2 HRI

NGC 3923 was observed with the HRI for 45 ks from 10–17 January 1995 and for 26 ks from 22–26 June 1995. Both observations were positioned at the field center where the PSF is smallest (David et al. 1997). For detailed explanation of our reduction of HRI data we refer the reader to the related study of NGC 720 by Buote & Canizares (1996b).

We restricted the data to those in pulse-height analyzer (PHA) bins 2–8 since they maximized the S/N of the data of each observation. For each observation we binned the events into images with $1''$ pixels to optimize determination of ellipticities within a $30''$ radius of the galaxy center (§4). Exposure maps were generated with the standard software for each image and then used to flatten the images.

An accurate aspect solution is critical to analysis of isophote shapes with the HRI on small scales ($r \lesssim 15''$), with the amplitude of the asymmetrical distortion due to incomplete aspect correction typically being most important for ($r \sim 5'' - 10''$) (David et al. 1997). The S/N of each of the NGC 3923 observations are too small to usefully perform the aspect correction algorithm of Morse (1995). The low S/N also makes it difficult to make strong statements about the ellipticity of isolated point sources indicative of aspect error. As a result, following Buote & Canizares (1996b) we search for possible aspect errors by examining the positions of point sources for each of the OBIs; i.e. the time intervals during which the spacecraft continuously pointed on the target.

Three OBIs contain most of the “on time” of the January observation: 19 ks for OBI-6, 20 ks for OBI-11, and 9 ks for OBI-14; 28 ks is distributed fairly evenly among 12 other OBIs. Using OBI-11 as a reference, the bright point sources in the NGC 3923 field are displaced by $2'' \pm 1''$ for OBI-6, and $3'' \pm 1.5''$ for OBI-14. These shifts, though statistically significant, are very consistent with the expected aspect uncertainties for a typical observation. To register all of the OBIs to one coordinate frame, we binned together those OBIs that were observed close together in time; i.e. OBIs 1–5, 6–9, 10–11, 12–13, and 14–15. Once registered to

the same coordinate frame, the images were all added. (Note that the image for each of these OBI groups was binned as above.)

The June observation proved to be problematic because none of the 19 OBIs had a long enough exposure to provide very accurate source positions. Hence, we were unable to perform a reliable test of the aspect solution. In order to make some estimate of the error, we grouped those OBIs closest together in time: OBIs 1–3, 4–12, 13–16, and 17–19. For three of these groups, less than $1''$ shifts were required, but the OBI 4–12 group required an $8'' \pm 1''$ shift. This large shift is questionable since all but one source was too faint to even obtain a centroid measurement using the alignment software in IRAF.

As it is unclear from considerations of the OBIs how accurate is the aspect error for the June observation, we compared the ellipticity and orientations (computed as described in §4) of the surface brightness with those of the January observation. Unfortunately, we find significant disagreement between the two observations; note the disagreement occurs whether or not we include the OBIs 4–12 for the June observation. In particular, the position angles determined from the January observation are fully consistent with the PSPC data and the optical position angles for $r \lesssim 30''$, which agrees with NGC 720 and NGC 1332 (Buote & Canizares 1996a,b); the ellipticities are also consistent with the PSPC data. The June observations, however, have position angles that differ by over 60° and the ellipticities, particularly for $r \gtrsim 20'' - 30''$ are less than 0.1 as opposed to ~ 0.25 for the January observation. Furthermore, the radial profile (see §5) of the June observation is significantly flatter for $r \lesssim 10''$.

Thus, the isophote shapes and orientations are inconsistent for the two observations. The differences point to a serious aspect error in the June observations. That is, although we would expect aspect error to induce ellipticity in an intrinsically circular source, if the distortion occurs nearly along the minor axis of a moderately elliptical source, it will *reduce* the ellipticity of the source, as well as alter the position angle. The flatter inner radial profile of the June data is

Table 1. Identified Point Sources

Source	R. A.	Decl.
1	11 ^h 51 ^m 06 ^s	-28° 46' 47"
2	11 50 58	-28 43 58
3	11 50 15	-28 53 22
4	11 51 04	-28 57 30
5	11 51 29	-28 43 51
6	11 51 33	-28 47 41
7	11 51 35	-28 56 23
8	11 51 40	-28 46 24
NWa	11 50 53	-28 47 04
NWb	11 50 58	-28 46 30

These sources (expressed in J2000 coordinates) were identified from visual inspection of the PSPC image within a 10' radius of the galaxy center. They were removed from the image for spatial analysis as described in §3.

also consistent with uncorrected wobble. As a result, we do not include the June data in our analysis. (This is not critical since the S/N to be gained over the 45 ks is marginal.)

We display the reduced January observation in Figure 1.

3 POINT SOURCES

It is readily apparent from inspection of Figure 1, particularly for the higher S/N PSPC data, that the X-ray emission of NGC 3923 is significantly contaminated by foreground/background point sources. Within a 10' radius of the galaxy center at least 8 point sources are easily identified by visual inspection of the PSPC image. (Only $r \lesssim 3'$ is shown in the Figure.) We list the positions of these sources in Table 1.

For our analysis of the isophote ellipticities and orientations (§4) and the radial profile (§5) of the X-ray surface brightness, we wish to analyze only the distribution of the diffuse emission associated with NGC 3923 and thus these contaminating sources must be removed. The most important contaminating source is number (1) (which lies along the optical major axis to the N-E) since it lies closest to the galactic center where the S/N, and thus constraints on the surface brightness, are best; this source is also apparent in the HRI image. Next in importance is the extended emission approximately 2.5' to the N-W along the optical minor axis which appears to consist of emission from at least two point sources. These candidate sources are listed as NWa,b in Table 1.

Our preferred method for removing sources, which is well suited for analyzing quadrupole moments of X-ray images (Buote & Tsai 1996), is to first choose an annulus around each source to estimate the local background. Then a second order polynomial surface is fitted to the background which then replaces the source. We removed sources 2-8 using this method, but sources (1) and NWa,b require some elaboration.

Since source (1) affects ellipticity measurements for $r \gtrsim 100''$ we examined how robust the ellipticity and position angle were to the method used to remove the source. Another method to remove sources is by “symmetric substitution” (see Strimple & Binney 1979; Buote & Tsai 1995; Buote & Canizares 1996a). This method exploits the as-

sumed symmetry of the hot gas distribution. If the gas is approximately ellipsoidal, then we can replace source (1) with the corresponding emission obtained by reflecting the source over the galactic center; i.e. essentially on the other side of the major axis ($a \rightarrow -a$). Fortunately, we find that the ellipticities and position angles are virtually the same whether we remove source (1) by subtracting a model for the local background or by symmetric substitution. (We use the former method for ensuing analysis.)

The emission associated with NWa,b cannot be so easily removed because it is extended, and it is not obvious how to define a background model. Fortunately this emission only begins to affect the ellipticities for semi-major axes $\gtrsim 120''$. At these distance the S/N does not allow accurate constraints. However, this emission does need to be removed from the radial profile, and thus we iterate the local background method to remove the emission associated with NWa,b. This method is suitable for the radial profile since the azimuthal averaging is not overly sensitive to small non-axisymmetric residuals. (We mention the effect of removing this emission on the radial profile in §5.)

4 X-RAY ISOPHOTE SHAPES AND ORIENTATIONS

As is typical for current X-ray data of early-type galaxies the small number of counts (~ 1000) for the PSPC and HRI images of NGC 3923 implies that we can only hope to measure with any precision the ellipticity and position angle of the aggregate X-ray surface brightness in a large aperture. The method we employ is an iterative procedure (Carter & Metcalfe 1980) and is analogous to computing the two-dimensional moments of inertia within an elliptical region where the ellipticity, ϵ_M , is given by the square root of the ratio of the principal moments and the orientation of the principal moments gives the position angle, θ_M (see Buote & Canizares 1994 for application to ROSAT images). The parameters ϵ_M and θ_M are good estimates of the ellipticity (ϵ) and position angle (θ , or P.A.) of an intrinsic elliptical distribution of constant shape and orientation. For a more complex distribution ϵ_M and θ_M are average values weighted heavily by the outer parts of the regions.

We estimate the uncertainties on ϵ_M and θ_M using a Monte Carlo procedure described in Buote & Canizares (1996b). In sum, the procedure involves constructing 1000 realizations of the PSPC and HRI images taking into account statistical noise and unresolved sources; these unresolved sources are modeled according to the $\log N(> S) - \log S$ distribution given by Hasinger et al. (1993) and their profiles are given by the appropriate PSPC or HRI PSF. The 90% confidence limits on ϵ_M , for example, are defined by the 5th and 95th percentile values computed from the 1000 simulations.

The profiles of ϵ_M and θ_M are listed for the PSPC in Table 2 and for the HRI in Table 3. We also display the ϵ_M profiles and their 68% uncertainties in Figure 2. The apertures listed in the tables are chosen so that each increment in semi-major axis a consists of approximately 100 source

Table 2. PSPC Ellipticities and Position Angles

a (arcsec)	ϵ_M	68%	90%	θ_M	68%	90%	Counts
30.....	0.10	0.04-0.19	0.03-0.22	42	19-55	11-77	1116
40.....	0.12	0.09-0.15	0.07-0.17	25	15-41	07-53	1331
50.....	0.07	0.05-0.12	0.03-0.13	31	20-52	09-66	1460
60.....	0.08	0.05-0.15	0.03-0.19	57	38-81	26-101	1564
75.....	0.15	0.12-0.19	0.09-0.21	51	42-58	36-65	1670
90.....	0.15	0.11-0.20	0.06-0.23	48	37-60	31-71	1754
110.....	0.10	0.08-0.16	0.05-0.19	39	26-61	13-156	1870

The values of ϵ_M (and confidence limits) are computed within an aperture of semi-major axis a on the image with the background included; the counts, however, have the background subtracted. The values of θ_M are given in degrees N through E.

Table 3. HRI Ellipticities and Position Angles

a (arcsec)	ϵ_M	68%	90%	θ_M	68%	90%	Counts
12.....	0.25	0.13-0.32	0.08-0.39	69	44-83	30-92	309
17.....	0.26	0.14-0.31	0.08-0.36	59	50-76	43-88	412
23.....	0.22	0.09-0.27	0.05-0.32	66	47-81	34-102	506
32.....	0.13	0.07-0.21	0.04-0.26	63	35-82	15-107	631
44.....	0.14	0.11-0.27	0.07-0.31	76	41-87	31-103	735
60.....	0.16	0.10-0.28	0.05-0.33	74	44-101	33-123	825

See Table 2.

counts. We restrict the PSPC profile to $a \leq 110''$ because of contamination from sources NWa,b (see §3)[†].

The values of ϵ_M for the HRI have considerably larger estimated uncertainties than for the PSPC. In their regions of overlap, the HRI and PSPC give consistent ellipticities. For the smallest $a \lesssim 20''$, the HRI gives some indication of large ellipticity, $\epsilon_M \gtrsim 0.20$, but the 90% lower limits are less than 0.10; at these radii residual aspect errors could be important. At these a the PSPC is blurred by the PSF, but at $a \sim 70'' - 90''$ (~ 10 kpc) the PSPC gives the best constrained ellipticity for either the HRI or PSPC of $\epsilon_M \approx 0.15 \pm 0.05$. Although significant, this ϵ_M is less than that measured on similar scales for NGC 720 (~ 0.25 ; Buote & Canizares 1994; 1996b) and for NGC 1332 (~ 0.20 ; Buote & Canizares 1996a).

Like NGC 1332, the P.A. profiles of the PSPC and HRI data are consistent with the optical value of $\sim 49^\circ$ (Jedrzejewski 1987), albeit within the rather large uncertainties. Moreover, the PSPC P.A. for $a \gtrsim 90''$ may be affected by the bright source (1) and NWa,b (see Table 1), and thus it would be premature to rule out a P.A. twist like that in NGC 720 until higher resolution, better S/N data (e.g. AXAF) is obtained.

Finally, over the region $a \leq 110''$ we find no obvious

asymmetries in the (PSPC or HRI) surface brightness (Figure 1) suggestive of unresolved sources or environmental effects like ram pressure or tidal distortions; e.g. the centroids of the apertures are very steady over the semi-major axis listed in Tables 2 and 3. We also have divided up the region $r \leq 75''$ into quadrants (aligned with the major axis of NGC 3923) and have found the counts in each quadrant to be consistent with each other within $(1-2)\sigma$ errors, similar to the agreement seen for NGC 720 (Table 2 of Buote & Canizares 1996b).

5 RADIAL PROFILE OF X-RAY SURFACE BRIGHTNESS

In order to construct the azimuthally averaged radial profiles for the PSPC and HRI data we require measurements of their respective background levels. We selected annular regions centered on the galaxy that are sufficiently far from the galaxy center so that contamination from the galaxy is minimal. (Also, any point sources were removed.) We obtain a background rate of 2.4×10^{-4} cnts s^{-1} arcmin $^{-2}$ for the PSPC and a rate of 3.3×10^{-3} cnts s^{-1} arcmin $^{-2}$ for the HRI.

We binned the radial profiles so that each bin had approximately the same S/N. However, for the innermost bins the S/N is larger because we did not oversample the respective PSFs. The centers of the radial bins for both the PSPC and HRI data were determined by the centroid of the circular region containing $\sim 80\%$ of the total flux; in neither case did this choice critically affect the radial profile shape. We display the radial profiles in Figure 3 along with the PSFs; note that residuals of the emission near sources NWa,b may be seen in the PSPC profile for $r \sim 130'' - 150''$. The X-ray emission is clearly extended for both data sets.

[†] We emphasize that the bright point source (1) (see Table 1 and Section 3) does not affect the ellipticity measurements for $a \leq 90''$; i.e. we also measure $\epsilon_M = 0.15$ for $a = 75'', 90''$ on the image including source (1). However, the values at larger radii differ considerably depending on whether the source is removed or not; e.g. at $a = 120''$, we obtain $\epsilon_M = 0.3$ with the source and $\epsilon_M = 0.1$ without the source. As a result, when comparing model ellipticities to data in future sections of this paper we use only the ellipticities for $a \leq 90''$ which are robust to the inclusion or exclusion of source (1).

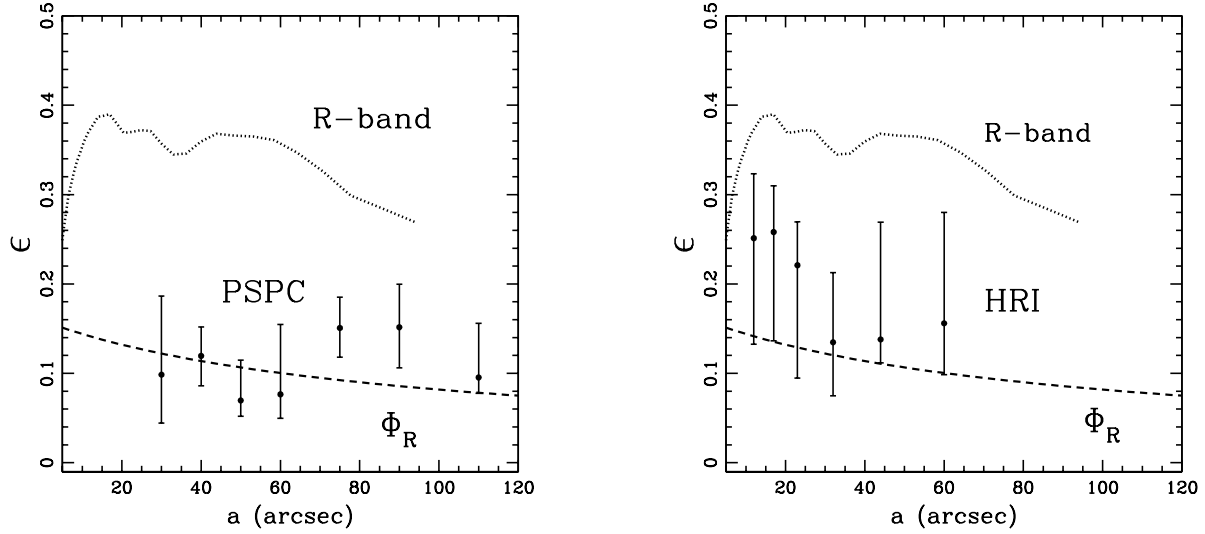


Figure 2. Moment ellipticities and 1σ errors for PSPC (left) and HRI (right) data. The isophotal ellipticities of the R -band light from Jedrzejewski (1987) are indicated by the dotted line. The dashed line represents the isopotential ellipticities of, Φ_R , the potential assuming $M \propto L_R$ (see §7).

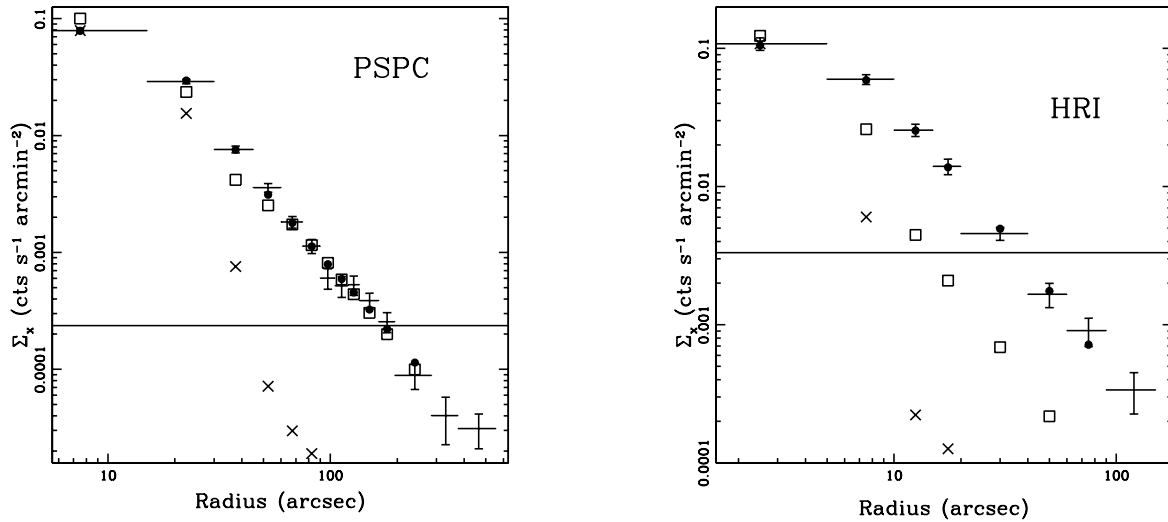


Figure 3. Radial surface brightness profiles of the PSPC (left) and HRI (right) data. The error bars indicate the data and the horizontal lines through each point show the bin sizes. The solid horizontal lines across each plot indicate the background level. The best-fit β model (filled circles), the PSFs (crosses), and the R -band light convolved with the respective PSFs (boxes) are also shown. All of these quantities have been binned as the X-ray data.

A convenient parametrisation of the X-ray radial profiles of early-type galaxies is given by the “ β model”, $\Sigma_x \propto (R_c^2 + R^2)^{-3\beta+0.5}$ (Cavaliere & Fusco-Femiano 1976). The model assumes that the gas is isothermal and that the stars, considered as test particles, follow a King law. Although these assumptions are unlikely to be strictly valid for ellipticals, this model provides a reasonable description of the *ROSAT* radial profiles of both NGC 720 (Buote & Canizares 1996b) and NGC 1332 (Buote & Canizares 1996a) as well as many other galaxies (e.g. Forman et al. 1985). Moreover, for *ROSAT* data the β model typically gives fits of quality very similar to more sophisticated mass models and thus it serves as a good benchmark for these more general models (as in §8).

Table 4. Simple β Model Fits to Radial Profile

Data	R_c (arcsec)	β	χ^2	dof	χ^2_{red}
PSPC	$5.6^{+1.1}_{-1.0}$	$0.47^{+0.02}_{-0.02}$	8.9	9	1.0
HRI	$5.1^{+1.6}_{-1.2}$	$0.46^{+0.05}_{-0.04}$	1.4	4	0.4
PSPC + HRI	$5.4^{+0.8}_{-0.8}$	$0.46^{+0.02}_{-0.01}$	10.7	15	0.7

The best-fit values and 90% confidence limits on one interesting parameter are listed for R_c and β . The PSFs of each data set have been incorporated into the fits.

In Table 4 we list the results of fitting the β model (convolved with the appropriate PSF) to the X-ray data;

NGC 3923 -- PSPC

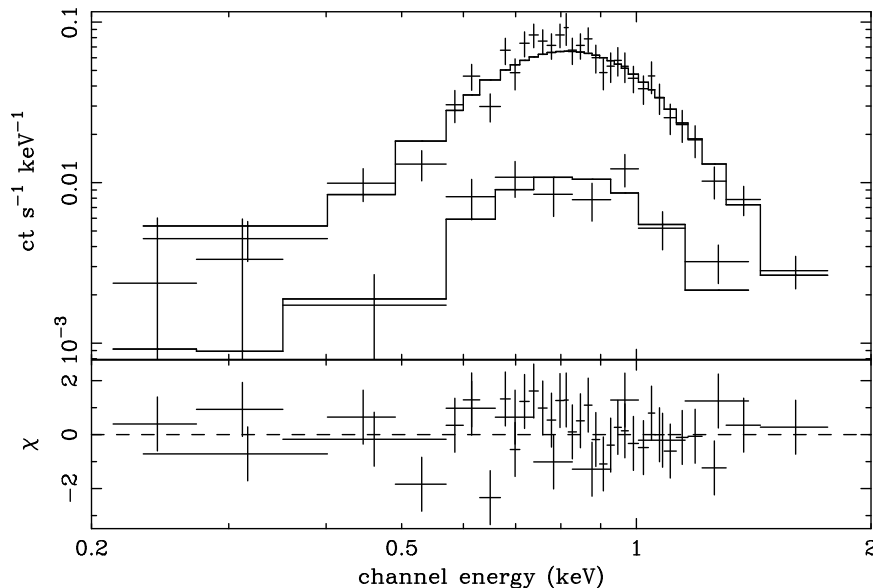


Figure 4. Absorbed single-temperature MEKAL model fit jointly to the inner (upper curve) and outer (lower curve) regions (see §6). Only the June, 1993 data is shown.

only those bins with $S/N \gtrsim 5$ were included in the fits. When fitted separately to the PSPC and HRI data, the β model gives a good quality fit and the derived R_c and β parameters are similar; note that if the emission from sources NWa,b is not removed from the PSPC data, the parameters of these fits are essentially unaffected but the value of χ^2 increases to 17.4.

The best-fit model obtained from jointly fitting the PSPC and HRI data is shown in Figure 3. The β model provides a reasonably good fit over a large radius range for both data sets. For comparison, we plot the R -band data from Jedrzejewski (1987) in Figure 3. We have binned the optical data like the X-rays and have convolved with the appropriate PSFs; for radii larger than the limiting $a = 103''$ of Jedrzejewski, we extrapolate the data using the best-fitting De Vaucouleurs model. For radii larger than the PSFs, the shape of the optical profile, Σ_R , is very similar to the shape of Σ_x in agreement with expectations from steady-state cooling flow models (e.g. Sarazin 1987). However, the X-ray and optical profiles disagree markedly for small radii ($r \lesssim 10''$) with Σ_R being much more centrally peaked than Σ_x . Because of its smaller PSF this effect is more pronounced in the HRI data.

In particular, it is clear that a population of discrete X-ray sources distributed like Σ_R cannot contribute significantly to the emission. If we assume that the hot gas is described by a β model or related model (see §8) then adding such a discrete component only worsens joint fits to the PSPC and HRI data. We find that $f_{hg}/f_{disc} > 3.6$ (90% confidence), where f_{hg} is the flux of the hot-gas component (β model) and f_{disc} is the flux of the discrete sources where the 0.4-2 keV flux is computed within a circle of $r = 2'$.

Spectral analysis of ASCA data of NGC 3923 by Buote & Fabian (1997) shows that two temperature models are required by the data with a cold component, $T_C = 0.55$ keV, and a hot component, $T_H = 4.2 (> 2.2)$ keV (90% confi-

dence); the ratio of the 0.5-2 keV flux of the cold component to the hot component is 1.9 (1.3-2.8) at 90% confidence. If the discrete sources are indeed distributed like Σ_R , then the emission of the hot component cannot be entirely due to discrete sources. This would indicate that the emission of the hot component is actually largely due to another phase of the hot gas and that T_H is overestimated due to an artifact of fitting low S/N data as suggested by Buote & Fabian. (Note that the cold-to-hot flux ratio derived by Buote & Fabian in the 0.5-2 keV band remains essentially the same when computed in the 0.4-2 keV band analyzed in our paper.)

6 SPECTRAL ANALYSIS

Spectral analysis of the X-ray data is required for our study of the mass distribution in NGC 3923 to determine (1) how much of the emission is due to hot gas, and (2) the temperature profile of the gas. The superior spectral resolution of ASCA is better suited than ROSAT to address issue (1), and as discussed at the end of the previous section, the ASCA spectrum is consistent with $\sim 35\%$ of the X-ray emission in the 0.5-2 keV band arising from a population of discrete sources (Buote & Fabian 1997). Since this much discrete emission is inconsistent with the ROSAT radial profiles we shall neglect it and assume all of the emission arises from hot gas. This assumption does not seriously affect analysis of the mass distribution if the discrete contribution is $\lesssim 20\%$ (Buote & Canizares 1997a).

Unlike the ASCA data, the ROSAT PSPC data allows us to directly measure any temperature gradients. To investigate this issue we analyzed the PSPC spectra in a circular region with $r = 30''$ and an annular region with $r = 60'' - 120''$; the spectra of these regions are shown in Figure 4. We fit a model consisting of Galactic absorption ($N_H = 6.4 \times 10^{20} \text{ cm}^{-2}$ - Stark et al. 1992) and a thin

Table 5. Spectral Fits

Name	T (keV)	Z (Z_{\odot})	χ^2	dof	χ^2_{red}
0'' – 30''	$0.50^{+0.05}_{-0.04}$	$0.44^{+2.3}_{-0.15}$	51.3	50	1.0
60'' – 120''	$0.53^{+0.17}_{-0.15}$	$0.09^{+0.67}_{-0.07}$	7.9	12	0.6
BOTH	$0.50^{+0.04}_{-0.05}$	$0.45^{+1.2}_{-0.16}$	61.6	64	1.0

Results of fitting a MEKAL model modified by Galactic photo-electric absorption. We list 90% confidence limits on one interesting parameter.

thermal plasma. Our thermal plasma model is the MEKAL model which is a modification of the original MEKA code (Mewe, Gronenschild, & van den Oord 1985; Kaastra & Mewe 1993) where the Fe-L shell transitions crucial to the X-ray emission of ellipticals have been re-calculated (Liedahl et. al 1995). We take solar abundances according to Anders & Grevesse (1989) and photo-electric absorption cross sections according to Balucińska-Church & McCammon (1992).

All of the spectral fitting was implemented with the software package XSPEC (Arnaud 1996) using the χ^2 minimization method. In order for the weights to be valid for the χ^2 method we regrouped the PI bins such that each group contained at least 20 counts. We restricted the fits to energies above 0.2 keV because of the low S/N coupled with uncertainties in the PSPC response at these lowest energies. We fitted the December and June observations jointly, but with their normalizations as free parameters.

The results of the spectral fits are given in Table 5. The model is an excellent fit to the low resolution PSPC data in both regions with the temperatures and abundances giving consistent values within the uncertainties. There is some indication that the inner region prefers higher abundances than the outer region. This may suggest a real abundance gradient, or it may be due to a difference in S/N (Buote & Fabian 1997). In any event, a joint fit to the inner and outer region is formally acceptable and gives parameters similar to the inner region. Hence, we find no evidence of temperature gradients, and since the PSPC spectral constraints are even tighter than found for NGC 720 any gradients consistent with this data are unimportant for analysis of the mass distributions (see Buote & Canizares 1994).

Note that we did jointly fit the PSPC and ASCA data and found that the constraints did not change appreciably from the ASCA results alone, even for two-temperature models.

7 GEOMETRIC TEST FOR DARK MATTER

The shapes of the X-ray isophotes allow the shape and radial distribution of gravitating matter to be probed in a way that is more robust than the traditional spherical approach (for a review see Buote & Canizares 1997b). Assuming the hot gas is approximately in hydrostatic equilibrium and that the emission is adequately described by a single phase, then the volume X-ray emissivity, j_x , obeys an ‘‘X-ray Shape Theorem’’ (Buote & Canizares 1994, §3.1; 1996a, §5.1) which states that j_x and the gravitational potential, Φ , have the same three-dimensional shapes independent of the temperature profile of the gas. One may thus make a ‘‘Geometric

Test’’ for dark matter that is distributed differently from L (with L the luminosity distribution of the optical stellar light) by comparing the shape of Φ_L generated assuming $M \propto L$ with the shape of j_x obtained from deprojecting the X-ray image data. As this comparison is independent of the poorly constrained temperature profile, $T(r)$, of the gas (see §6) this test for dark matter is more robust than computing the radial mass distribution which is directly proportional to $T(r)^{\ddagger}$.

NGC 3923 has negligible stellar rotation, but if rotation of the gas is dynamically important then we must replace Φ with the appropriate effective potential. Theoretically, even without strong stellar rotation one may (Kley & Mathews 1995) or may not (Nulsen et al. 1984) expect a rotating cooling flow to develop depending on whether angular momentum of the gas is conserved. Highly flattened X-ray isophotes indicative of a cooling disk have not been observed in ellipticals and thus we shall ignore any contribution from gas rotation[§].

To apply the Geometric Test we constructed a constant M/L potential using the R -band surface photometry, Σ_R , of Jedrzejewski (1987). The major-axis profile of Σ_R is well fitted by a De Vaucouleurs Law with an effective semi-major axis, $a_e = 92''$. Taking into account the ellipticity of the isophotes, we fitted the De Vaucouleurs Law to the mean radial profile, where the mean radius is, $r = \sqrt{ab} = a\sqrt{q}$, where a is the major axis and q the axial ratio. This gives a mean effective radius, $R_e = 73''$. Since the 3-D density giving rise to a De Vaucouleurs Law is well approximated by the Hernquist profile, $\rho \propto r^{-1}(r_s + r)^{-3}$ (Hernquist 1990), we consider for our $M \propto L_R$ model a Hernquist profile with $r_s = R_e/1.8153 = 40''$. Furthermore, we take ρ to be stratified on oblate or prolate spheroids of constant ellipticity, where we use the intensity weighted ellipticity of Σ_R , $\langle \epsilon_R \rangle = 0.30$.

This simple prescription for the $M \propto L_R$ model is sufficient for comparison to the ROSAT X-ray data because of the relatively crude X-ray constraints: i.e. only a global constraint on the isophote shapes of the PSPC data over a small range in radius, $r \sim 70'' - 90''$, is useful for the comparison – as we show below, the HRI data do not provide interesting constraints over the PSPC data. With better quality data from future missions which accurately measure ellip-

[‡] The X-ray shape analysis is also more robust to the effects of multi-phase gas and magnetic fields – see Buote & Canizares (1997b).

[§] We should also emphasize that the wiggles displayed by the smoothed X-ray isophotes in Figure 1 are not statistically significant and thus do not suggest departures of the gas from hydrostatic equilibrium; i.e. the S/N of the PSPC and HRI data is too poor to measure deviations of isophote shapes from elliptical. However, even if those wiggles in the contours were due to real non-equilibrium motions in the gas, the hydrostatic assumption is still very likely a good one. Buote & Tsai (1995) analyzed the X-ray isophotes of an X-ray cluster formed in an N-body/hydrodynamical simulation. They concluded that relatively soon after major mergers the cluster settled down quickly to a relaxed state which allowed accurate determination of the shape of the mass from analysis of the X-ray isophote shapes, even though the simulated clusters had X-ray isophotes far from elliptical in shape.

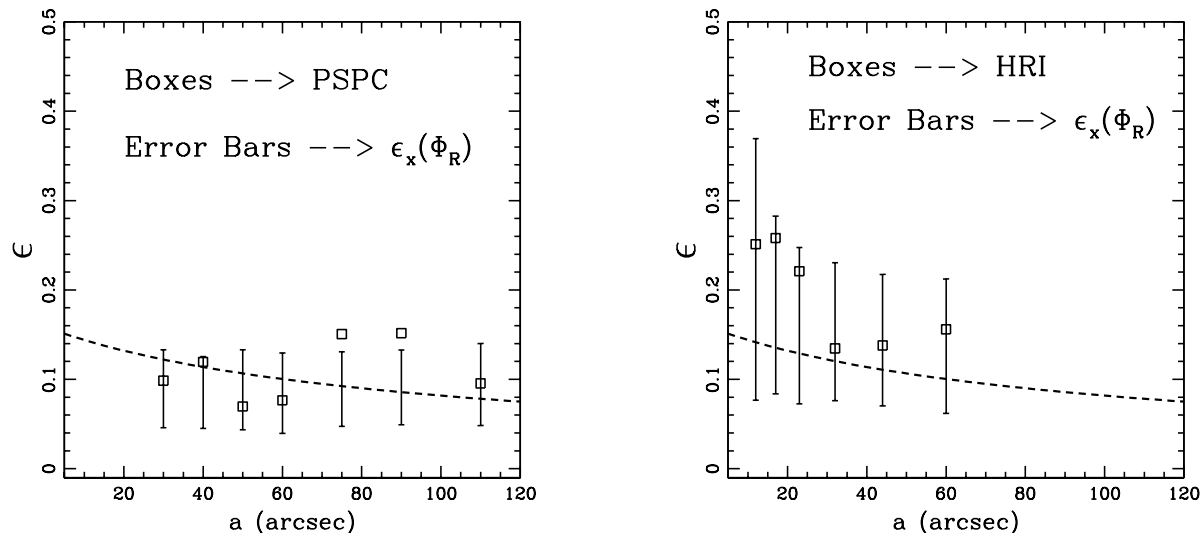


Figure 5. Geometric Test for Dark Matter – see §7.

ticity gradients over a large range in radius a more accurate $M \propto L_R$ approximation will need to be considered.

We show in Figure 2 the ellipticities of the isopotential surfaces of the potential, Φ_R , assuming $M \propto L_R$ and edge-on oblate symmetry. These ellipticities are considerably smaller than those of the R -band light because the spherically symmetric monopole term in the potential dominates the isopotential ellipticities for $r \gtrsim r_c$ [¶]. The ellipticities of the X-ray surface brightness, particularly for the PSPC data for $a \sim 70'' - 90''$, appear to be significantly larger than the isopotential ellipticities and thus indicate a failure of the $M \propto L_R$ hypothesis.

However, to rigorously compare Φ_R to the X-ray data we must formally deproject Σ_x to get the ellipticities of j_x . The procedure we adopt for this comparison, which is suitable for the relatively crude constraints provided by the X-ray data, is to first fit a simple model to the radial profile of Σ_x ; for this purpose, the results of the β model fit jointly to the PSPC and HRI data are suitable (see §5). This model for $\Sigma_x(R)$ is then deprojected to obtain $j_x(r)$ ^{||}. We then assign to j_x the ellipticities of Φ_R which gives a spheroidal emissivity distribution, $j_x(r, \theta)$. This spheroidal j_x is then projected back onto the sky plane, while adjusting R_c and β to maintain a best fit of the radial profile of Σ_x (convolved with the appropriate instrument PSF), to yield a $M \propto L_R$ model of the X-ray surface brightness. We compute moment ellipticities, $\epsilon_x(\Phi_R)$, for 1000 Monte Carlo simulations of this model in analogy to the data (see §4).

The 1σ error bars for $\epsilon_x(\Phi_R)$ as well as the observed X-ray ellipticities and the 3-D isopotential ellipticities of Φ_R are displayed in Figure 5. Although most of the measured X-ray ellipticities lie within the error bars, the best measured PSPC ellipticities from $a \sim 70'' - 90''$ exceed the values predicted by the edge-on oblate Φ_R at the 85% confidence

level. The edge-on prolate Φ_R is formally discrepant at the 80% level at these radii^{**}.

Hence, the X-ray isophote shapes indicate that the $\epsilon_x(\Phi_R)$ model is either too round, too centrally concentrated, or both; i.e. dark matter is required which is flattened and probably more extended than Σ_R . This discrepancy, though formally marginal and of lesser significance than found for the other two early-type galaxies studied NGC 720 and NGC 1332 (e.g. Buote & Canizares 1997a,b), is of precisely the same character: i.e. flattened and extended dark matter is required in these ellipticals. Since the flattest optical isophotes of NGC 3923 are rounder than those of NGC 720 and NGC 1332, it is possible that the symmetry axis of NGC 3923 is inclined more along the line-of-sight than the other two. This would account for the marginal

^{**} We caution that interpretation of the significance of this discrepancy must take into account the *PSPC* PSF as we have done; i.e. the two deviant data points for $a \sim 75'' - 100''$ are not simply random fluctuations weighted equally with other points over the radial range investigated. (Also, care is required in the interpretation of the last measured ϵ_M at $a = 110''$ for the *PSPC* data since its value depends on the bright point source that is removed – see Sections 3 and 4.) This point is illustrated in Figures 13 (a) and (b) of Buote & Canizares (1996a) for a similar X-ray analysis of NGC 1332. That is, the X-ray ellipticity profiles produced by different models are smeared out by the *PSPC* PSF, and thus a discrepancy is only achieved at radii large enough so that the ellipticity differences between models exceeds the relatively large error bars of the measured ellipticity; of course, the radial range is limited from above by the decreasing S/N. Thus, the radii $a \sim 75'' - 100''$ are where the different models convolved with the *PSPC* PSF begin to show significant ellipticity differences and the X-ray data still have good constraints on the measured ellipticity. NGC 3923, NGC 1332, and NGC 720 are quite similar in this regard since they have similar length scales and similar S/N *PSPC* observations. However, the *HRI* data of NGC 720 are of sufficient quality so that the effect of the PSFs on the Geometric Test can be clearly seen: see Figure 2 of Buote & Canizares (1997b).

[¶] See Figure 2-13 in §2.3 of Binney & Tremaine (1987) for a related discussion of isopotential ellipticities.

^{||} Note that the parameters in Table 4 correspond to the deprojected parameters.

significance of the NGC 3923 result if the intrinsic shapes of the three galaxies are in fact similar.

We note that, as explained in Section 5.1 of Buote & Canizares (1996a), if an ellipsoidal galaxy is inclined along the line of sight, then the Geometric Test results give a lower limit to the true discrepancy. That is, if mass follows light, then j_x and Φ_L must be co-axial and thus share the same inclination angle, i . Since the projection of an ellipsoid with $i < 90^\circ$ is necessarily rounder than if the galaxy were viewed edge-on, deprojection of Σ_x and Σ_L assuming $i = 90^\circ$ will yield j_x and Φ_L which are rounder than in reality. However, this edge-on deprojection of an inclined ellipsoidal galaxy only means that any differences in the inferred shapes of j_x and Φ_L are smaller than if the true inclination angle were used.

8 DETAILED HYDROSTATIC MODELS

The results of the Geometric Test from the previous section suggest the presence of a dark matter halo that is flattened and more extended than the optical light. To generally constrain the allowed distribution of gravitating matter, we must employ explicit solutions of the hydrostatic equation. As the low S/N of the PSPC and HRI images does not justify a sophisticated non-parametric inversion of the data, we instead consider simple intuitive models to place constraints on the aggregate shape and radial distribution of gravitating mass. As in our previous studies (e.g. Buote & Canizares 1997b), we follow the pioneering approach of Binney & Strimple (1978) and solve the hydrostatic equation assuming a single-phase, non-rotating, ideal gas,

$$\tilde{\rho}_g = \exp \left[\Gamma (1 - \tilde{\Phi}) \right], \quad (1)$$

where $\Gamma = \mu m_p \Phi(0) / k_B T$ and where, e.g. $\tilde{\rho}_g = \rho_g(\vec{x}) / \rho_g(0)$. Equation (1) assumes the gas is isothermal, but Strimple & Binney (1979) and others (Fabricant, Rybicki, & Gorenstein 1984; Buote & Canizares 1994; Buote & Tsai 1995) have shown that the constraints on the shape of the gravitating matter distribution are not very sensitive to temperature gradients. Hence, we shall assume an isothermal gas which is consistent with the spectral constraints for NGC 3923 (§6) and the temperature profiles of other galaxies (e.g. Buote & Canizares 1994; for a review see Sarazin 1997).

Our procedure begins with a model for the gravitating mass. We consider spheroidal density distributions whose isodensity surfaces are concentric, similar spheroids. By examining oblate and prolate configurations we bracket the intermediate behavior of triaxial models; i.e. as our important constraints on the models are the X-ray isophote shapes for semi-major axes $a \sim 75''$, the detailed radial behavior of the isophote shapes and orientations which distinguish triaxial models cannot be usefully constrained by the NGC 3923 PSPC and HRI data.

Once the type of density model and its associated ellipticity, ϵ_{mass} , are chosen, we compute Φ and ρ_g . (We initially focus on one-component models of the density of the gravitating matter and then consider separate density models for the dark and luminous matter.) The model X-ray surface brightness is then generated by integrating ρ_g^2 along the

line of sight^{††} assuming the galaxy is viewed edge-on^{‡‡}. We model the radial mass as either a softened isothermal potential with mass density, $\rho \propto (a_s^2 + a^2)^{-1}$, or a Hernquist profile, $\rho \propto a^{-1}(a_s + a)^{-3}$, where a_s is the appropriate mass scale length in each case. These models bracket the interesting range of densities in our previous X-ray analyses of NGC 720 and NGC 1332^{§§}. We convolve the surface brightness with the PSF of the appropriate detector and evaluate the model on a grid of pixels identical to that used for analyzing the data (§2). We construct the radial profiles as for the data (§5) and determine a_s and Γ by fitting the model profile jointly to the PSPC and HRI data. (The normalizations of the PSPC and HRI are free parameters.) By comparing the ellipticity of the model surface brightness to the data we constrain the input ellipticity of the gravitating mass.

In Table 6 we give the constraints on the shape of the gravitating matter obtained from these models. The mass is significantly flattened, $\epsilon_{mass} \approx 0.5$, with the derived shapes being essentially the same for both the $\rho \sim r^{-2}$ and Hernquist models. These ellipticities are inconsistent with the intensity-weighted ellipticity of the R -band light ($\langle \epsilon_R \rangle = 0.30$) at more than the 90% level and are marginally inconsistent with the flattest optical isophotes ($\langle \epsilon_R^{max} \rangle = 0.39$). The derived range of values of ϵ_{mass} and the fact that they exceed the average ellipticity of the optical isophotes are consistent with the previous results we obtained for NGC 720 (and NGC 1332) (e.g. Buote & Canizares 1997a,b).

In Figure 6 we plot the radial profiles of typical $\rho \sim r^{-2}$ and Hernquist models. The $\rho \sim r^{-2}$ model fits are very similar in quality to those of the β model (§5) but with slightly larger values of χ^2 . (The differences are not obvious from visual inspection.) However, the Hernquist fits are noticeably worse than the $\rho \sim r^{-2}$ model and have unacceptable $\chi_{red}^2 \approx 1.9$. For $r \lesssim 15''$ the Hernquist model is too flat and then too steep out to $r \sim 100''$. At larger radii, the small fitted values of $\Gamma \sim 5.8$ force the Hernquist radial profile to be flatter than the data.

These deviations of the Hernquist model are most pronounced for the $M \propto L_R$ model (see §7) which has $a_s = 40''$ and a best-fit $\Gamma = 5.5$ and $\chi^2 = 56.0$ (16 dof). The PSPC ellipticities of the $M \propto L_R$ model are 0.07 for $a \sim 70'' - 90''$ which is below the 90% confidence limits of the data (Table 2). Hence, by assuming the gas is isothermal we find that the $M \propto L_R$ model is inconsistent with the data at a significance level greater than indicated by the more robust Geometric Test (§7).

It should be emphasized that most of the disagreement between the $\rho \sim r^{-2}$ and Hernquist models occurs in the in-

^{††} The plasma emissivity is a very weak function of temperature when convolved with the spectral response of either the PSPC or HRI.

^{‡‡} We assume the symmetry axis of the galaxy spheroid lies in the plane of the sky; i.e. we are not attempting in this analysis to uncover the true three-dimensional shape, though Binney & Strimple (1978) have found that the X-ray analysis is not extremely sensitive to small inclination of the symmetry axis with respect to the sky plane. See Buote & Tsai (1995) for a thorough discussion of projection effects on X-ray shape analysis.

^{§§} The Hernquist density gives fits to the density profiles of halos in Cold Dark Matter simulations that are very similar to the universal model of Navarro et al. (1997).

Table 6. Ellipticity of the Gravitating Matter

Model	Oblate ϵ_{mass}		Prolate ϵ_{mass}		a_s (arcsec)	$ \Gamma $	χ^2	dof	χ^2_{red}
	68%	90%	68%	90%					
$\rho \sim r^{-2}$	0.43-0.59	0.35-0.65	0.40-0.54	0.33-0.58	2.2-3.1	6.6-7.2	16	15	1.1
Hernquist	0.45-0.61	0.36-0.66	0.42-0.55	0.33-0.59	53-75	5.7-5.8	28	15	1.9

Derived shapes of the gravitating matter for the spheroidal mass models assuming an isothermal gas (see §8). 90% confidence ranges are quoted for the scale length a_s and $|\Gamma|$. Typical values of χ^2 are listed in the 90% intervals. Note for the $M \propto L_R$ model we obtain $\chi^2 = 56.0$ for 16 dof.

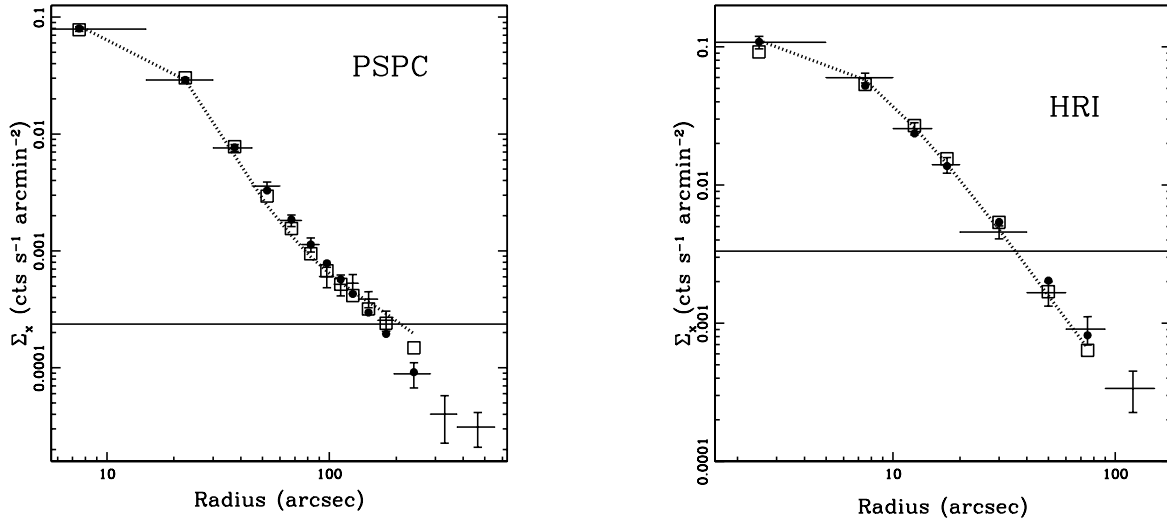


Figure 6. Radial surface brightness profiles of selected oblate models fit to the PSPC (left) and HRI (right) data. The error bars indicate the data and the horizontal lines show the bin sizes. The filled circles represent the best-fit $\rho \sim r^{-2}$ model having $\epsilon_{mass} = 0.50$; the boxes represent the best-fit Hernquist model with $\epsilon_{mass} = 0.50$; the dotted line is the best-fitting constant M/L model. The radial profiles of these models have been binned as the X-ray data.

nermost bins. For example, if we exclude the two inner bins for the PSPC ($r = 0'' - 30''$) and the three inner bins for the HRI ($r = 0'' - 15''$)^{¶¶} we obtain a minimum χ^2 of ~ 10.0 for the $\rho \sim r^{-2}$ model and $\chi^2 \sim 11.4$ for the Hernquist model. Since in these innermost regions the surface brightness profile could be modified by a multi-phase cooling flow or by magnetic fields, we suggest some caution in interpreting χ^2 values of our models in these central regions until better data can distinguish between different scenarios.

However, there is reason for optimism on both of these accounts. The distortion due to a multi-phase cooling flow is likely to be insignificant since single-phase analyses generally provide good descriptions for multi-phase cooling flows in the cores of clusters (Thomas, Fabian, & Nulsen 1987; Allen, Fabian, & Kneib 1996). Since no significant radio emission has been detected from NGC 3923 (e.g. Birkinshaw & Davies 1985) it is unlikely that the hot gas is supported by magnetic fields. It should also be added that the $\rho \sim r^{-2}$ model appears to fit the radial profile better than the Hern-

quist model for $r \sim 100'' - 300''$, but the effect is not highly significant because of the low S/N in this region^{|||}.

If we fit the $M \propto L_R$ model and add dark matter following the $\rho \sim r^{-2}$ model, the fits are marginally improved over the single-component case with a minimum $\chi^2 = 13.3$ obtained for a ratio $M_{DM}/M_R = 10$ and $M_{DM}/M_R > 3$ (90% confidence). The ellipticity of the dark matter, ϵ_{DM} , is essentially that of ϵ_{mass} for $M_{DM}/M_R = 10$ but increases systematically so that $\epsilon_{DM} \approx \epsilon_{mass} + 0.10$ at the lower limit $M_{DM}/M_R = 3$. Here it should be understood that M_{DM} includes only dark matter that is distributed differently from L_R and that the χ^2 values from the radial profile fits for given ratios M_{DM}/M_R depend on the assumed temperature profile.

The Hernquist profiles are only affected when $M_{DM}/M_R \sim 1$ at which point the fits are improved to minimum $\chi^2 \sim 21$ with large $a_s \sim 400''$. The dark matter in these models is required to be extremely flattened.

Similar to our analysis of the β model (§5), we find that adding a discrete component with X-ray emission proportional to L_R does not improve the fits for the $\rho \sim r^{-2}$ model; we place a slightly stricter limit of $f_{hg}/f_{disc} > 4.5$

^{¶¶} We remove a larger region for the PSPC because of its larger PSF.

^{|||} Note that the limits on ϵ_{mass} are essentially unaffected when the central bins are excluded.

(90% confidence). The Hernquist models are actually improved by the addition of a discrete component such that $\chi_{\text{red}}^2 = 1.2$ for $f_{hg}/f_{disc} = 4.6$. However, essentially all of this improvement takes place for the central bins discussed above; i.e. if we exclude those bins from the fits, then the discrete model does not improve the fits significantly. Hence, a discrete component distributed like L_R does not improve fits to Σ_x with the $\rho \sim r^{-2}$ model, and the improvement observed for the Hernquist model occurs in the central bins for which other physics (e.g. multi-phase cooling flows, magnetic fields) may equally affect the models.

In Table 7 we give the spherically averaged masses corresponding to the models in Table 6. We only quote masses at a few interesting radii to emphasize that without precise constraints on the temperature profile (and only an aggregate constraint on the isophote shapes) we do not really constrain the detailed mass profile. (Note that the spectral constraints in §6 which indicate an approximate isothermal gas apply only for $r \lesssim 15h_{70}^{-1}$ kpc.) The masses of the $\rho \sim r^{-2}$ and Hernquist models agree very well within $10h_{70}^{-1}$ kpc as expected because over much of this region the large scale lengths of the Hernquist model imply an approximate logarithmic slope of -2. Assuming the gas to be isothermal out to $r > 50h_{70}^{-1}$ kpc, the $\rho \sim r^{-2}$ model, with its flatter slope, has approximately twice the mass of the Hernquist model at that distance. The gas mass is less than 1% of the gravitating mass over the entire radius range investigated.

Using the total *B*-band luminosity from Faber et al. (1989) scaled to 30 Mpc, $L_B = 3.45h_{70}^{-2} \times 10^{43}$ erg cm⁻² s⁻¹ = $6.95h_{70}^{-2} \times 10^{10} L_{\odot}$, we have that the *B*-band mass-to-light ratio in solar units is $\sim 5h_{70}M_{\odot}/L_{\odot}$ at $10h_{70}^{-1}$ kpc for the $\rho \sim r^{-2}$ and Hernquist models. At $r = 50h_{70}^{-1}$ kpc, the $\rho \sim r^{-2}$ model has $M/L_B \sim 32h_{70}M_{\odot}/L_{\odot}$ while the Hernquist model has $M/L_B \sim 17h_{70}M_{\odot}/L_{\odot}$. These M/L_B values within $10h_{70}^{-1}$ kpc are very consistent with stellar dynamical studies of ellipticals (e.g. van der Marel 1991). The larger (extrapolated) M/L_B values at $50h_{70}^{-1}$ kpc agree with previous X-ray studies of ellipticals (e.g. Sarazin 1997) indicating that NGC 3923 has a mass distribution typical for a galaxy of its luminosity.

9 CONCLUSIONS

We have analyzed the gravitating matter distribution of the E4 galaxy NGC 3923 using archival X-ray data from the *ROSAT* PSPC and HRI. Analysis of the PSPC data, which allows more precise constraints than the HRI data, demonstrates that the X-ray isophotes are significantly elongated with ellipticity $\epsilon_x = 0.15(0.09 - 0.21)$ (90% confidence) for semi-major axis $a \sim 10h_{70}^{-1}$ kpc and have position angles aligned with the optical isophotes within the estimated uncertainties. A bright point source located $\sim 100''$ along the major axis inhibits reliable ellipticity constraints for larger radii.

By applying a ‘‘Geometric Test’’ for dark matter, which essentially compares the shapes of the observed X-ray isophotes to those predicted if mass traces the optical light L (independent of the poorly constrained temperature profile of the gas), we found that the ellipticity of the PSPC X-ray surface brightness exceeds that predicted by the constant M/L hypothesis at the 80%-85% confidence level. The

‘‘Geometric Test’’ result is conservative since it only considers signatures of dark matter that are distributed differently from the optical light.

Although the evidence for dark matter from the Geometric Test is marginal, the results from models which employ an explicit solution of the hydrostatic equation assuming an isothermal gas (which is supported by the PSPC spectrum – §6) indicate that $M \propto L$ is highly inconsistent with the radial profiles of the PSPC and HRI data ($\chi_{\text{red}}^2 = 3.5$ for 16 dof). This particular discrepancy arises because L is too centrally concentrated: the derived scale length of the gravitating matter is approximately 1.5-2 times that of L . The ellipticities predicted by this $M \propto L$ model fall below the PSPC data at a significance slightly greater than the 90% level. Modeling the gravitating mass with a density run $\rho \sim r^{-2}$ or with a Hernquist profile we find that the ellipticity of the gravitating matter is, $\epsilon_{mass} \cong 0.35 - 0.65$ (90% confidence), which is larger than the intensity weighted optical ellipticity (ϵ) = 0.30.

This evidence for dark matter which is more flattened and more extended than L is similar to our conclusions from previous X-ray studies of two other ellipticals, NGC 720 and NGC 1332, but at somewhat smaller significance level than for NGC 720 (e.g. Buote & Canizares 1997b). These results are consistent with analyses of known gravitational lenses (e.g. Keeton, Kochanek, & Falco 1997), two polar ring galaxies (Sackett et al. 1994; Sackett & Pogge 1995), and flaring disks in spiral galaxies (e.g. Olling 1996). The ellipticities of the gravitating matter derived from our X-ray analyses and these other methods are consistent with those of halos produced by CDM simulations (e.g. Dubinski 1994).

If an isothermal gas is assumed then models with matter density $\rho \sim r^{-2}$ are favored over Hernquist models (and similar models like the universal CDM profile of Navarro et al. 1997). For $r \sim 100'' - 300''$ the $\rho \sim r^{-2}$ model marginally fits the data better than the Hernquist model. However, most of the difference in these models occurs in the central radial bins where the effects of multi-phase cooling flows, magnetic fields, and discrete sources could affect the surface brightness profiles, though we have argued the effects are unlikely to be important (see §8). (The derived shape of the gravitating mass is mostly robust to these issues – Buote & Canizares 1997b.) This support for nearly r^{-2} profiles agrees with previous studies of gravitational lenses (e.g. Maoz & Rix 1993; Kochanek 1995), although a recent paper finds that density profiles with changing slopes (e.g. Hernquist and NFW) are preferred (Williams 1997).

An emission component that is proportional to L cannot contribute significantly to the *ROSAT* X-ray emission of NGC 3923, and thus discrete sources should not affect our constraints on the gravitating matter (Buote & Canizares 1997a). However, the *ASCA* spectral data when fitted with two thermal components yield a cold component, $T_C = 0.55$ keV, and a hot component, $T_H \sim 4$ keV, where the relative flux of cold-to-hot is ~ 1.9 in the *ROSAT* band (Buote & Fabian 1997). The conventional interpretation of the hot component (e.g. Matsumoto et al. 1997; Loewenstein & Mushotzky 1997) is that it arises from discrete sources. But our analysis (§5) shows that $\sim 35\%$ of the 0.5-2 keV emission cannot be distributed like the optical light which would be expected of discrete sources. Hence, either the emission from discrete sources is not distributed like L , or the hot compo-

Table 7. Gravitating Mass and Gas Mass

Model	$5h_{70}^{-1}$ kpc	$10h_{70}^{-1}$ kpc	$50h_{70}^{-1}$ kpc
$\rho \sim r^{-2}$	$(1.1 - 2.8) \times 10^{11} h_{70}^{-1} M_{\odot}$	$(2.4 - 6.0) \times 10^{11} h_{70}^{-1} M_{\odot}$	$(12.2 - 30.5) \times 10^{11} h_{70}^{-1} M_{\odot}$
Hernquist	$(1.3 - 3.3) \times 10^{11} h_{70}^{-1} M_{\odot}$	$(2.6 - 7.1) \times 10^{11} h_{70}^{-1} M_{\odot}$	$(6.0 - 18.1) \times 10^{11} h_{70}^{-1} M_{\odot}$
Gas	$0.14 \times 10^9 h_{70}^{-5/2} M_{\odot}$	$0.45 \times 10^9 h_{70}^{-5/2} M_{\odot}$	$6.4 \times 10^9 h_{70}^{-5/2} M_{\odot}$

90% confidence values of the gravitating mass corresponding to the oblate and prolate models in Table 6 which include 90% uncertainties in the (isothermal) temperature. The statistical errors on the gas mass are less than 10%.

nent obtained from the spectral fits cannot be entirely due to discrete sources as suggested by Buote & Fabian (1997).

The constraints we have obtained for NGC 720, NGC 1332, and now NGC 3923 from analyses of their X-ray isophote shapes and radial surface brightness profiles provide an initial demonstration of the power of X-ray analysis for probing the shape and radial distribution of gravitating matter in early-type galaxies. The next generation of X-ray satellites, particularly *AXAF* and *XMM*, have the capability to accurately map X-ray isophote shapes and orientations from the cores ($r \sim 1''$) out to 10s of kpc for many galaxies***. The spatially resolved spectra provided by these future missions will allow more precise constraints on temperature gradients and the contribution from discrete sources. Thus, unlike most other methods, obtaining interesting X-ray constraints on the shape and radial density profile of the gravitating matter will be possible for a large sample of early-type galaxies since the X-ray analysis is applicable to any isolated early-type galaxy whose soft X-ray emission ($\sim 0.5 - 2$ keV) is dominated by hot gas.

REFERENCES

Allen S. W., Fabian A. C., Kneib J.-P., 1996, MNRAS, 279, 615
 Anders E., Grevesse N., 1989, Geochimica et Cosmochimica Acta, 53, 197
 Arnaud K., 1996, in Jacoby G. and Barnes J., eds., Astronomical Data Analysis Software and Systems V, ASP Conf. Series volume 101, p17
 Aschenbach B., 1988, Appl. Opt., 27(8), 1404
 Balucińska-Church M., McCammon D., 1992, 400, 699
 Binney J., Strimble O., 1978, MNRAS, 185, 473
 Binney J., Tremaine S., 1987, Galactic Dynamics. Princeton Univ. Press, Princeton
 Birkinshaw M., Davies R. L., 1985, ApJ, 291, 32
 Brighenti F., Mathews W. G., 1997, ApJ, 486, L83
 Broeils A., 1997, in D. Zaritsky ed., UC Santa Cruz Workshop on Galactic Halos, ASP Conf. Series, in press
 Buote D. A., Canizares C. R., 1994, ApJ, 427, 86
 Buote D. A., Canizares C. R., 1996a, ApJ, 457, 177
 Buote D. A., Canizares C. R., 1996b, ApJ, 468, 184
 Buote D. A., Canizares C. R., 1997a, ApJ, 474, 650
 Buote D. A., Canizares C. R., 1997b, in D. Zaritsky ed., UC Santa Cruz Workshop on Galactic Halos, ASP Conf. Series, in press (astro-ph/9710001)
 Buote D. A., Fabian A. C., 1998, MNRAS, in press, (astro-ph/9707117)

*** The vastly improved spatial resolution of *AXAF* over the *ROSAT* PSPC will allow easy exclusion of the bright point source (1) (see Table 1) which hindered the present analysis of NGC 3923.

Buote D. A., Tsai J. C., 1995, ApJ, 439, 29
 Buote D. A., Tsai J. C., 1996, ApJ, 458, 27
 Canizares C. R., Fabbiano G., Trinchieri G., 1987, ApJ, 312, 503
 Carter D., Metcalfe N., 1980, MNRAS, 191, 325
 Cavaliere A., Fusco-Femiano R., 1976, A&A, 49, 137
 David L. P., Jones C., Forman W., Daines S., 1994, ApJ, 428, 544
 David L. P., et al., 1997, The ROSAT High Resolution Imager (HRI) Calibration Report, (U.S. ROSAT Science Data Center - Smithsonian Astrophysical Observatory)
 de Zeeuw P. T., 1996, in Lahav O., Terlevich E., Terlevich R. J. eds., Gravitational Dynamics, Cambridge Contemporary Astrophysics, (Cambridge University Press: Cambridge)
 de Zeeuw P. T., 1997, in Arnaboldi M., Da Costa G. S., P. Saha, eds., The Nature of Elliptical Galaxies, Proceedings of the Second Stromlo Symposium, ASP Conference Series, in press (astro-ph/9704095)
 Dubinski J., 1994, ApJ, 431, 617
 Faber S. M., Wegner G., Burstein D., Davies R. L., Dressler A., Lynden-Bell D., Terlevich R. J., 1989, ApJS, 69, 763
 Fabricant D., Rybicki G., Gorenstein P., 1984, ApJ, 286, 186
 Forman W., Jones C., Tucker W., ApJ, 1985, 293, 102
 Gerhard O. E., Jeske G., Saglia R. P., Bender R., 1997, MNRAS, in press (astro-ph/9710129)
 Hasinger G., Turner T. J., George I. M., Boese G., 1993, MPE/OGIP Calibration Memo CAL/ROS/93-015
 Hasinger G., Burg R., Giacconi R., Hartner G., Schmidt M., Trümper J., Zamorani G. 1993, A&A, 275, 1
 Hernquist, L. 1990, ApJ, 356, 359
 Irwin J. A., Sarazin C. L., 1996, ApJ, 471, 683
 Jedrzejewski R., 1987, MNRAS, 226, 747
 Jones C., Stern C., Forman W., Breen J., David L., Tucker W., Franx M., 1997, ApJ, 482, 143
 Kaastra J. S., Mewe R., 1993, A&AS, 97, 443
 Keeton C., Kochanek C. S., Falco E., 1997, ApJ, submitted (astro-ph/9708161)
 Kim D.-W., Fabbiano G., 1995, ApJ, 441, 182
 Kim D.-W., Fabbiano G., Trinchieri G., 1992, ApJ, 393, 134
 Kley W., Mathews, W. G., 1995, ApJ, 438, 100
 Kochanek C. S., 1991, ApJ, 373, 354
 Kochanek C. S., 1995, ApJ, 445, 559
 Liedahl D. A., Osterheld A. L., Goldstein W. H., 1995, ApJ, 438, L115
 Loewenstein M., Mushotzky R. F., 1997, in D. Zaritsky ed., UC Santa Cruz Workshop on Galactic Halos, ASP Conf. Series, in press (astro-ph/9710339)
 Maoz D., Rix H.-W., 1993, ApJ, 416, 425
 Matsumoto H., Koyama K., Awaki H., Tsuru T., Loewenstein M., Matsushita K., 1997, ApJ, 482, 133
 Merritt D., Quinlan G. D., 1997, ApJ, submitted (astro-ph/9709106)
 Mewe R., Gronenschild E. H. B. M., van den Oord G. H. J., 1985, A&AS, 62, 197
 Milgrom M., 1983, ApJ, 270, 365
 Moore B., Governato F., Quinn T., Stadel J., Lake G. 1997, ApJ, submitted (astro-ph/9709051)

- Morse J. A., 1995, in E. M. Schlegel R. Petre eds., *The Soft X-ray Cosmos* (AIP Conf. Series 313), (AIP Press: New York), 252
- Navarro J. F., Frenk C. S., White S. D. M., 1997, *MNRAS*, in press
- Nulsen P. E. J., Stewart G. C., Fabian A. C., 1984, *MNRAS*, 208, 185
- Olling R. P., 1996, *AJ*, 112, 457
- Olling R. P., Merrifield M. R., in D. Zaritsky ed., *UC Santa Cruz Workshop on Galactic Halos*, ASP Conf. Series, in press (astro-ph/9710224)
- Ostriker J. P., 1993, *ARA&A*, 31, 689
- Pfeffermann E., et al., 1987, *Proc. SPIE*, 733, 519
- Rangarajan F. V. N., Fabian A. C., Forman W. R., Jones C., 1995, *MNRAS*, 272, 665
- Raymond J. C., Smith B. W., 1977, *ApJS*, 35, 419
- Rix H.-W., de Zeeuw P. T., Cretton N., van der Marel R. P., Carollo C. M., 1997, *ApJ*, 488, 702
- Romanowsky A. J., Kochanek C. S., 1997, *ApJ*, in press (astro-ph/9708212)
- Sackett P. D., Rix H.-W., Jarvis B., Freeman K. C., 1994, *ApJ*, 436, 629
- Sackett P. D., Pogge R. W., 1995, in E. M. Schlegel R. Petre eds., *The Soft X-ray Cosmos* (AIP Conf. Series 313), (AIP Press: New York), 141
- Sackett P. D., 1996, in C. S. Kochanek, J. N. Hewitt eds., *Gravitational Lensing* (IAU 173), (Dordrecht: Reidel), (astro-ph/9508098)
- Sarazin C. L., 1997, in Arnaboldi M., Da Costa G. S., and P. Saha, eds., *The Nature of Elliptical Galaxies*, Proceedings of the Second Stromlo Symposium, in press
- Schechter, P. L. 1987, in T. de Zeeuw ed., *Structure and Dynamics of Elliptical Galaxies* (IAU Symp. 127), (Dordrecht: Reidel), 217
- Stark A. A., Gammie C. F., Wilson R. W., Bally J., Linke R. A., Heiles C., Hurwitz M. 1992, *ApJS*, 79, 77
- Statler T. S., 1994, *AJ*, 108, 111
- Strimble O., Binney J., 1979, *MNRAS*, 185, 473
- Tanaka, Y., Inoue H., Holt S. S. 1994, *PASJ*, 46, L37
- Thomas P. A., Fabian A. C., Nulsen P. E. J., 1987, *MNRAS*, 228, 973
- Trinchieri G., Fabbiano G., Canizares C., 1986, *ApJ*, 310, 637
- Trinchieri G., Kim D.-W., Fabbiano G., Canizares C., 1994, *ApJ*, 428, 555
- Trümper J., 1983, *Adv. Space Res.*, 2, 241
- van der Marel, R. P., 1991, *MNRAS*, 253, 710
- Williams L. R., 1997, *MNRAS*, in press (astro-ph/9709283)